Supplementary Information for

Trap States and Charge Transport Mechanisms in Small Molecule TADF Materials with Different Donor-Acceptor Structures

Hongmin Hao,[a] Bangxiong Kang,[a] Shuxin Li,[a] Jinyu Lei,[a] Min Zheng[a], Yanxiang Cheng,[b] Quan Niu,[a*] and Yuguang Ma[a]

[a]*State Key Laboratory of Luminescent Materials and Devices, School of Materials Science and Engineering, South China University of Technology, Guangzhou 510640, P. R. China.*

[b]*State Key Laboratory of Polymer Physics and Chemistry, Changchun Institute of Applied Chemistry, Chinese Academy of Sciences, Changchun 130022, P. R. China.*

*e-mail: qqniu@scut.edu.cn

CONTENTS

1. Extended Gaussian Disorder Model (EGDM)

In 2005, Pasveer et al. proposed a charge-transport model that simultaneously accounts for the effects of electric field and charge-carrier density, known as the extended Gaussian disorder model (EGDM).[1] In this model, the carrier mobility is described as a function of temperature, electric field, and carrier concentration, thereby extending the original Gaussian disorder model. According to the EGDM, at room temperature and under low electric-field conditions, variations in charge-carrier mobility are primarily governed by the carrier concentration. In contrast, under low-temperature or high-electric-field conditions, the electric-field dependence becomes dominant. The charge-carrier mobility in the EGDM framework can be expressed as:

$$\mu(T,p,E) = \mu(T,p) \times f(T,E) \#(1)$$

here

$$\mu(T,p) = \mu_0 C_1 exp\left[-C_2\left(\frac{\sigma}{k_B T}\right)^2 + \frac{1}{2}\left(\left(\frac{\sigma}{k_B T}\right)^2 - \frac{\sigma}{k_B T}\right)\right](2pa^3)^{\delta} \#(2)$$

where δ is given by

$$\delta = 2\frac{ln\left(\left(\frac{\sigma}{k_B T}\right)^2 - \frac{\sigma}{k_B T}\right) - ln(ln4)}{\left(\frac{\sigma}{k_B T}\right)^2} \#(3)$$

The second term in the equation describes the dependence on the applied electric field *E*, which is given by

$$f(T,E) = exp\left[0.44\left(\left(\frac{\sigma}{k_B T}\right)^{\frac{3}{2}} - 2.2\right) \times \sqrt{1 + 0.8\left(\frac{Eea}{\sigma}\right)^2} - 1\right] \#(4)$$

In the limit of zero charge-carrier concentration and zero applied electric field, the carrier mobility in eqn (1) can be simplified to a temperature-dependent expression:

$$\mu_0(T) = \mu_0 C_1 exp\left[-C_2\left(\frac{\sigma}{k_B T}\right)^2\right] \#(5)$$

In the above equation, μ_0 is the mobility prefactor, and C_1=1.8×10^{-9} and C_2=0.42 are empirical constants.

It has been reported that the electron current is significantly lower than the hole current,[2] and this pronounced reduction in electron current is attributed to trap-limited conduction (TLC).

$$n_t(\xi) = \left(\frac{N_t}{k_B T_t}\right) exp\left(\frac{-E}{k_B T_t}\right) \#(6)$$

Here, $n_t(E)$ represents the density of trap states at energy E, N_t is the total trap density, $k_B T_t$ characterizes the energetic width of the trap distribution, E_c denotes the energy of the conduction band edge, and T_t is the characteristic temperature. When $T_t > T$, it can be approximated that $f(E)=1$ in the energy range $E<E_f$, while $f(E)=0$ for $E_f<E<$, where E_f is the Fermi level. Under this approximation, the concentration of trapped charge carriers is given by

$$n_t = \int_{E_f}^{\infty} \left(\frac{N_t}{k_B T_t}\right) exp\left(\frac{-E}{k_B T_t}\right) dE = N_t exp\left(\frac{-E_f}{k_B T_t}\right) = N_t \left(\frac{n}{N_c}\right)^{\frac{T}{T_t}} \#(7)$$

The densities of free charge carriers n and trapped charge carriers n_t are related by:

$$\frac{n}{N_t} = \left(\frac{n_t}{N_t}\right)^r \#(8)$$

Under the approximation $n<n_t$, by applying the boundary condition $V = \int_0^L F(x)d(x)$, one obtains

$$J = N_c e\mu \left(\frac{\varepsilon_0 \varepsilon_r}{e N_t}\right)^r \left[\left(\frac{2r+1}{r+1}\right)^{r+1} \left(\frac{r}{r+1}\right)^r\right] \frac{V^{r+1}}{L^{2r+1}} \#(9)$$

Here, $r=T_t/T$, and the effective density of states in the conduction band is estimated to be $N_c=2.5\times10^{19}$ cm^{-3}. According to eqn (9), the J-V characteristics of the device are determined by three parameters: the electron mobility μ_n, the trap density N_t, and the trap distribution parameter T_t.

2. Trap dilution theory

In 1962, Mark and Helfrich systematically investigated charge transport in materials containing an exponential distribution of trap energy levels and demonstrated the pronounced influence of trap-state distributions on carrier transport characteristics.[3] From the discrete energy level E_{tc} below the conduction band, the energetic width of the exponential trap distribution is characterized by the trap temperature T_t. Under these conditions, the relationship between the free carrier density n and the trapped carrier density n_t can be expressed as:

$$\frac{n}{N} = \left(\frac{n_t}{N_t e^{E_{tc}/kT_t}} \right)^r \#(10)$$

where N represents the density of transport sites, N_t is the trap density, T is the absolute temperature, $r=T_t/T$, and k is the Boltzmann constant. By combining eqn (10) with Poisson's equation, the following trap-limited current expression can be derived:

$$J = N_c q \mu_e \left(\frac{\varepsilon_0 \varepsilon_r}{q N_t e^{E_{tc}/kT_t}} \right)^r \left[\left(\frac{2r+1}{r+1} \right)^{r+1} \left(\frac{r}{r+1} \right)^r \right] \frac{V^{r+1}}{L^{2r+1}} \#(11)$$

Where N_c is the effective density of states, q is the elementary charge, μ_e is the free-electron mobility, $\varepsilon_0\varepsilon_r$ is the dielectric permittivity, V is the applied voltage, and L is the thickness of the sample.

For trap states exhibiting a Gaussian energy distribution within the bandgap, a similar trap-limited current expression can be derived, with the exponent r being related to the depth and width of the trap distribution.[4] In the case of a single shallow trap level, the trap-limited current is proportional to the ratio of the transport site density to the trap density N/N_t. In contrast, for systems containing an energetic distribution of trap states, the current scales with $(N/N_t)^r$.

Consequently, in semiconductors dominated by a single shallow trap level, simultaneous reduction of the transport site density N and trap density N_t (for example,

by diluting the semiconductor in an insulating matrix) does not significantly alter the trap effect. However, for deep traps or trap systems with a broad energetic distribution satisfying $r>1$, dilution markedly weakens the trapping effect. Taking a semiconductor with $r=4$ as an example, a simultaneous one-order-of-magnitude decrease in both N and N_t leads to an approximately three-orders-of-magnitude increase in the trap-limited current.[5] By mitigating electron trapping through trap dilution, a more balanced hole and electron transport within the device can be achieved, thereby enhancing the efficiency of electroluminescent devices.

3. Materials, Device fabrication, Electrical & EL characterization, Optical characterization, Electrochemical

BPAPTC, BPAMTC, AcPTC, PxPTC, and PtPTC were provided by Prof. Yanxiang Cheng's group at the Changchun Institute of Applied Chemistry, Chinese Academy of Sciences. bis(3,5-di(9H-carbazol-9-yl)phenyl)-diphenylsilane(SimCP2) and 1,3,5-tri[(3-pyridyl)phen-3-yl]benzene(TmPyPB) are purchased from Luminescence Technology Corporation as the doped host material and electrontransporting layer, respectively.

All OLEDs were fabricated on glass substrates coated with a patterned transparent ITO (indium tin oxide) conductive layer. The ITO glasses were cleaned by successively sonicating in a detergent solution, distilled water, acetone, and isopropanol in an ultrasonic bath. Prior to use, each ITO glass was cleaned by rinsing with acetone and isopropanol. Subsequently, the surface of the ITO substrate was dried for 30 min in an oven at 393 K. Then, the ITO substrates were treated by a Harrick Plasma PDC32G-2, 100W Plasma Cleaner for 10 min ozone plasma treatment. After that, PEDOT:PSS (CLEVIOS PVP AI 4083) was spin coated on pre-cleaned ITO substrates to form a 40 nm hole transport layer and baked at 100 °C for 30 minutes. Compounds BPAPTC (2 mg) and SimCP2 (8 mg, 99%, Acros) were dissolved in 1 mL Chlorobenzene to obtain

the required solution(take the 20% wt% ratio as an example, other doping ratios will adjust the proportion of BPAPTC and SimCP2 according to this concentration). The prepared mixtures filtered with a pore filter was spin coated at 1500 rpm for 120 seconds on PEDOT:PSS layer to form a 50 nm EML. LiF (1nm) and Al (100 nm) were successively deposited by the vacuum thermal evaporation (M. Braun MB-200MOD evaporation system integrated with M. Braun glove-box) under a base vacuum of about 5×10^{-7} mBar. The film thickness and deposition rate were monitored and controlled in situ by using an oscillating quartz thickness monitor.The evaporation rates for LiF and Al are , 0.2 Å/s and 1 Å/s, respectively. Single-carrier devices were fabricated using the same procedure as that for the OLEDs. Notably, for the electron-only devices, the ITO electrode was replaced by a 30 nm-thick Al layer, which was also deposited by physical vapor deposition.

Current density-voltage (*J-V*), luminance-voltage (*L-V*), current efficiency-current density, power efficiency-current density and external quantum efficiency-current density characteristics were measured with a Keithley 2400 Source Meter and a PhotoResearch SpectraScan PR-745 Colorimeter. The EQE and the power efficiency of OLEDs were calculated from the current density, the luminance, the EL spectra, and the angular distribution of the EL intensity. Transient PL decays and PL spectrum were measured with fluorescencephosphorescence spectrometer (FLS980, Edinburgh Instrument). UV-vis absorption spectra were recorded using a JASCO V-770 UV-vis-NIR spectrophotometer. All UV-vis absorption, PL spectra, and PL decay measurements were carried out on thin films at room temperature under a nitrogen atmosphere.

Electrochemical characterization was carried out using a CHI760D electrochemical workstation in a standard three-electrode configuration. ITO glass was used as the working electrode, a titanium plate (2 × 3 cm) as the counter electrode, and an Ag/Ag^{+} electrode (0.1 M $AgNO_3$ in acetonitrile) as the reference electrode. The supporting electrolyte was tetrabutylammonium hexafluorophosphate (0.1 M), and the concentration of the sample was 0.6 mg/mL in a mixed solvent of

dichloromethane/acetonitrile (v/v = 4:1). The measurements were performed in the potential range of 0-1.0 V with a scan rate of 100 mV/s. The HOMO energy levels were calculated according to the equation: $E_{HOMO} = -[E_{(onset,ox/Fc)} + 4.8]$ (eV).

4. Electrical and Optical Characterization

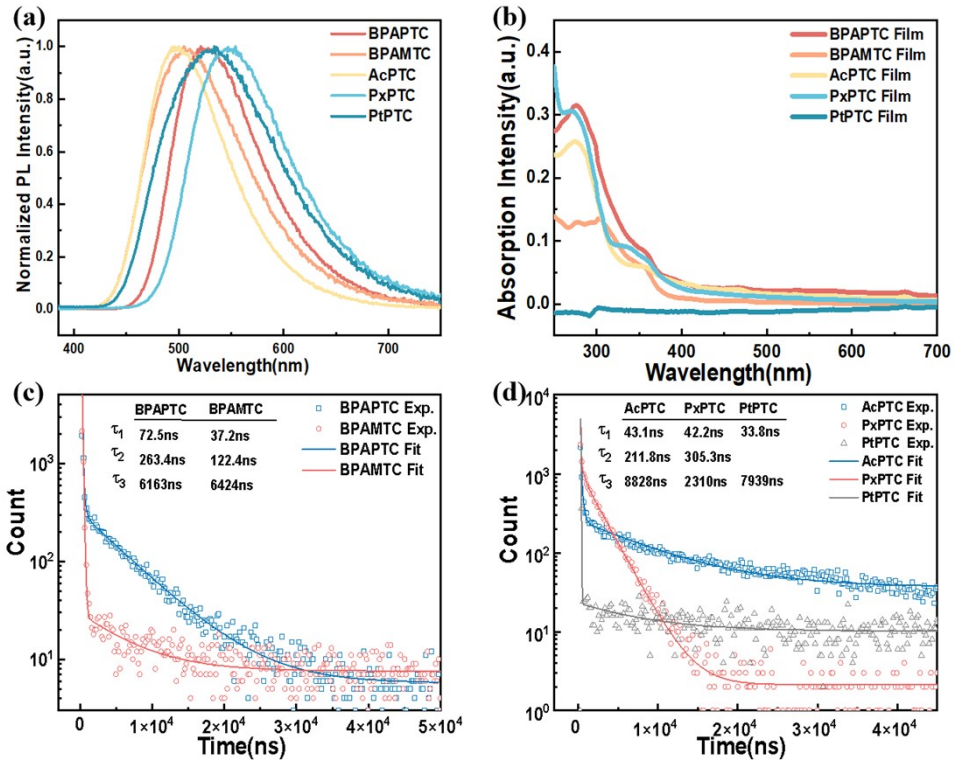

Figure S1. Photophysical Properties of BPAPTC, BPAMTC, AcPTC, PxPTC, and PtPTC: a) Fluorescence emission spectra; b) UV–visible absorption spectra; c, d) Time-resolved photoluminescence decay curves.

Table S1. Photophysical Parameters and Rate Constants of BPAPTC, BPAMTC, AcPTC, PxPTC, and PtPTC.

Film	PLQY [%]	τ_p[b] [ns]	τ_d[b] [ns]	Φ_p[c] [%]	Φ_d[c] [%]	k_p[d] [$\times10^6$s^{-1}]	k_d[e] [$\times10^5$s^{-1}]	k_{IC}[f] [$\times10^5$s^{-1}]	k_{ISC}[g] [$\times10^7$s^{-1}]	k_{RISC}[h] [$\times10^5$s^{-1}]	k_{nr} [$\times10^4$s^{-1}]	Φ_{ISC} [%]
BPAPTC[a]	90%	72.50	2178	8.10%	81.90%	1.12	4.13	1.24	1.26	3.72	8.72	91.00%
BPAMTC[a]	63%	43.97	136	18.90%	44.10%	4.30	46.40	25.20	1.59	29.20	444.00	70.00%
AcPTC[a]	73%	43.12	913	17.50%	55.50%	4.06	8.00	15.00	1.76	5.84	51.20	76.03%
PxPTC[a]	61%	42.22	2111	5.50%	55.50%	1.30	2.89	8.33	2.15	1.76	29.70	90.98%
PtPTC[a]	51%	33.79	7940	21.90%	29.10%	6.48	0.64	62.30	1.69	0.33	9.32	57.06%

[a] TADF films (30 nm) measured at 300 K; [b] Prompt fluorescence (τ_p) and delayed fluorescence (τ_d) lifetime components; [c] Prompt (Φ_p) and delayed (Φ_d) components of

photoluminescence quantum yield (PLQY); [d] Rate constant of the prompt component (k_p); [e] Rate constant of the delayed component (k_d); [f] Internal conversion rate constant (k_{IC}); [g] Intersystem crossing rate constant (k_{ISC}); [h] Reverse intersystem crossing rate constant (k_{RISC}).

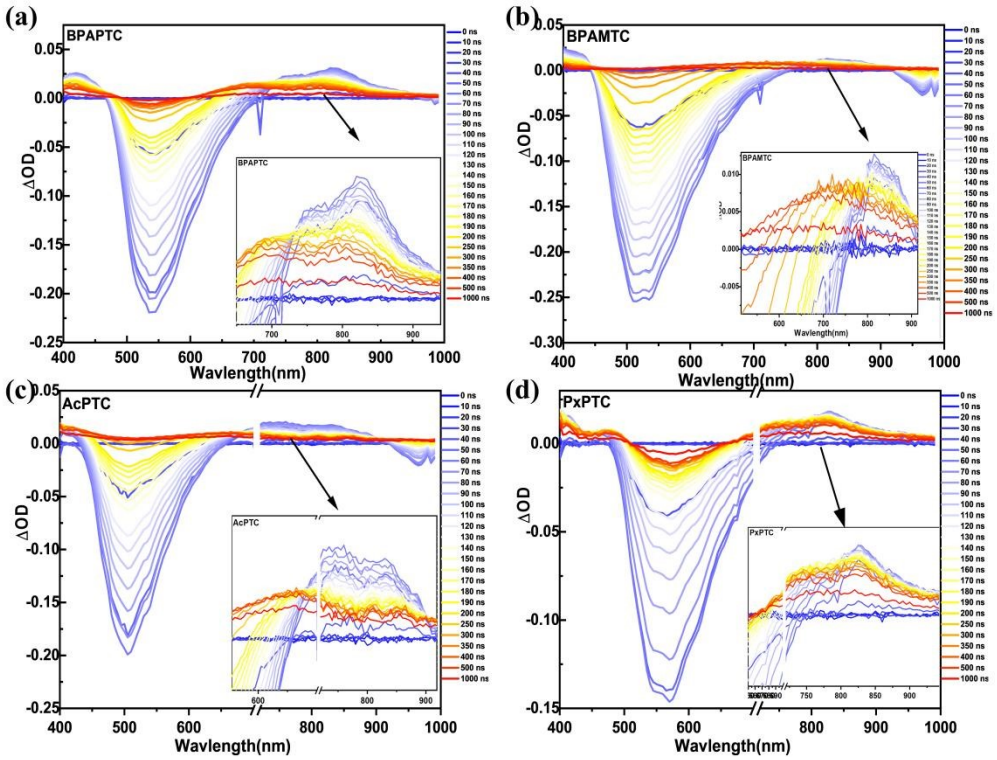

Figure S2. Nanosecond Transient Absorption Spectra of BPAPTC, BPAMTC, AcPTC, and PxPTC.

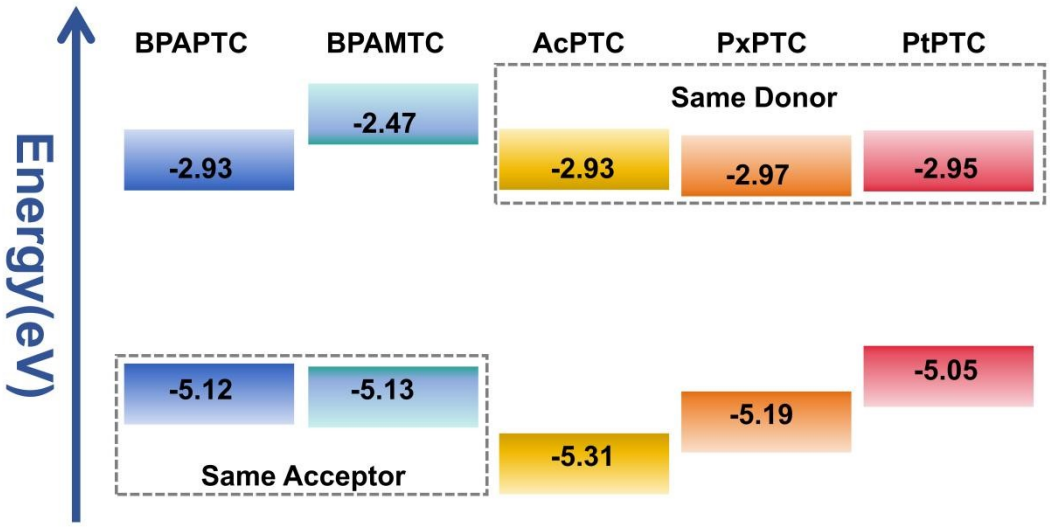

Figure S3. Schematic Energy Level Diagrams of TADF Materials with Different Donor-Acceptor Structures.

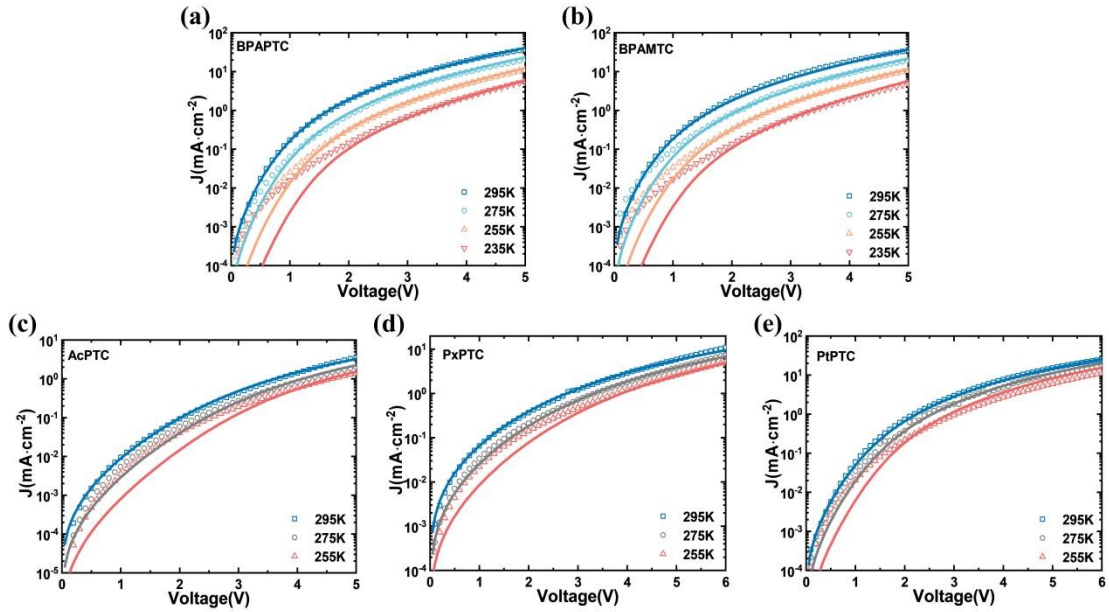

Figure S4. Temperature-Dependent Hole Transport *J-V* Characteristics of (a) BPAPTC, (b) BPAMTC, (c) AcPTC, (d) PxPTC, and (e) PtPTC (symbols represent experimental data; solid lines denote the fitting results based on the drift-diffusion model).

Table S2. Fitting parameters for hole transport of TADF materials with different donor-acceptor structures.

HOD Device	μ_0 [m^2/Vs]	a [nm]	σ_p [eV]	μ_{300K} [m^2/Vs]	P_t [cm^{-3}]	E_p [eV]
BPAPTC	27	2.2	0.09	2.90×10^{-10}	1.0×10^{17}	0.28
BPAMTC	18	2.2	0.09	1.99×10^{-10}	1.0×10^{17}	0.28
AcPTC	0.22	3.0	0.05	0.82×10^{-10}	1.5×10^{17}	0.31
PxPTC	0.27	3.0	0.05	1.01×10^{-10}	1.5×10^{17}	0.26
PtPTC	0.90	3.0	0.06	1.69×10^{-10}	1.0×10^{17}	0.33

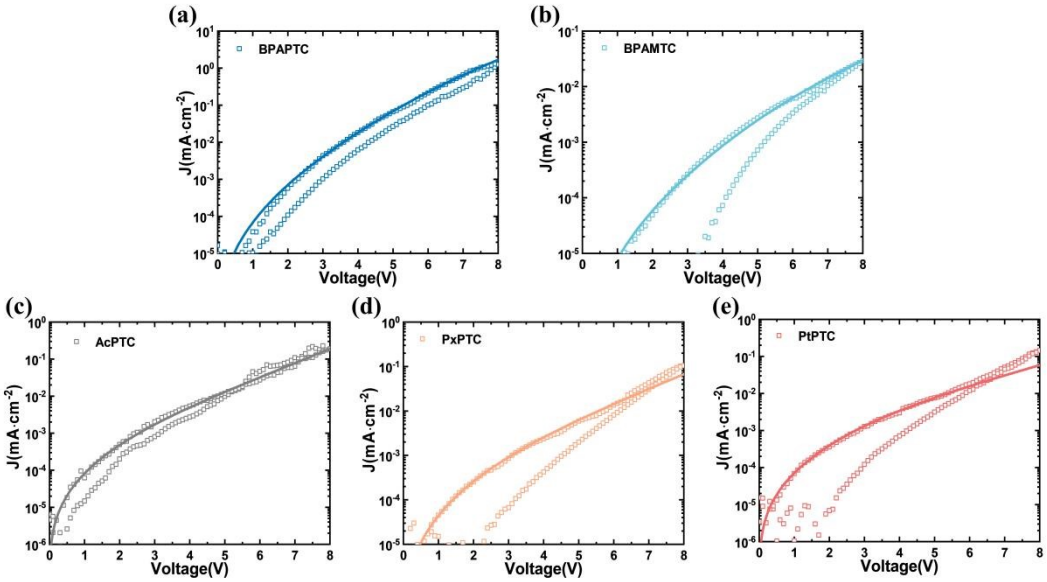

Figure S5. *J-V* Characteristics of electron-only devices for (a) BPAPTC, (b) BPAMTC, (c) AcPTC, (d) PxPTC, and (e) PtPTC (symbols represent experimental data; solid lines denote the fitting results based on the drift–diffusion model).

Table S3. Fitting parameters for electron transport of TADF materials with different donor-acceptor structures.

EOD Device	E_t [eV]	N_t [cm^{-3}]	σ_t [eV]
BPAPTC	0.30	5.7×10^{17}	0.15
BPAMTC	0.29	1.4×10^{24}	0.14
AcPTC	0.37	4.0×10^{17}	0.07
PxPTC	0.37	5.2×10^{17}	0.08
PtPTC	0.33	6.0×10^{17}	0.07

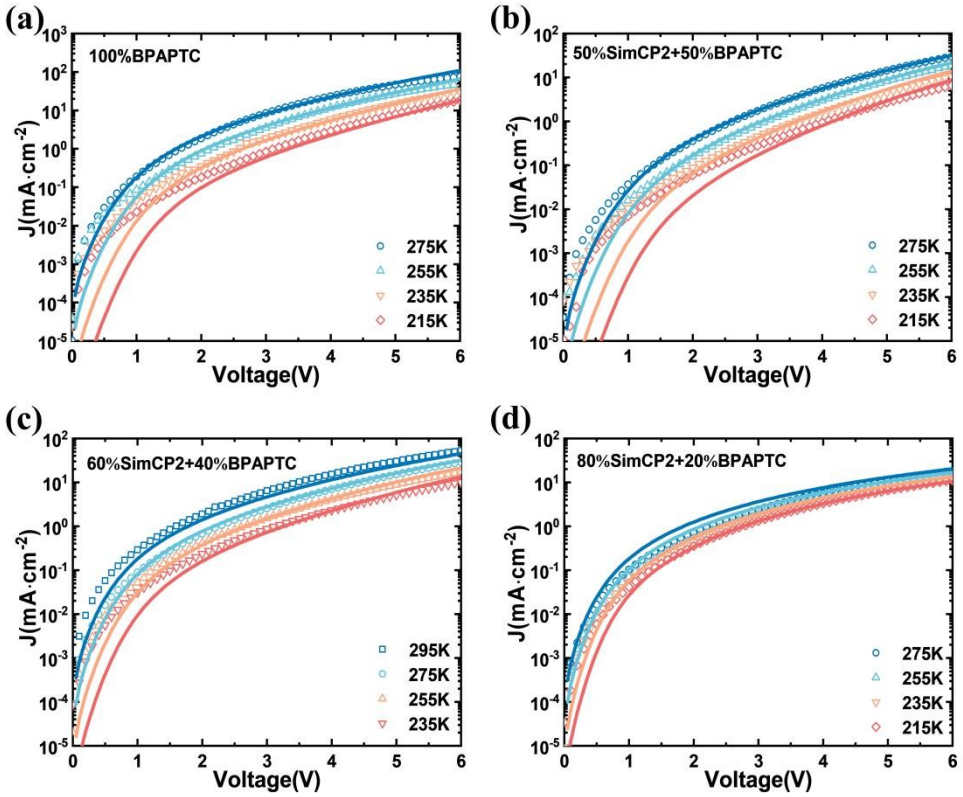

Figure S6. Temperature-Dependent J–V Characteristics of Single-Hole Devices with SimCP2+BPAPTC at Different Doping Ratios.

Table S4. Fitting parameters for hole transport of BPAPTC+SimCP2 with different doping ratios.

HOD Device	μ_0 [m^2/Vs]	a [nm]	σ_p [eV]	μ_{300K} [m^2/Vs]	P_t [cm^{-3}]	E_p [eV]
100 wt%BPAPTC	30	2.2	0.09	3.32×10^{-10}	1.0×10^{17}	0.28
50 wt%SimCP2+ 50 wt%BPAPTC	5.0	3.0	0.09	5.54×10^{-11}	1.0×10^{17}	0.28
60 wt%SimCP2+ 40 wt%BPAPTC	4.0	2.5	0.08	1.29×10^{-10}	0.8×10^{17}	0.28
80 wt%SimCP2+ 20 wt%BPAPTC	0.35	3.0	0.05	1.31×10^{-10}	0.7×10^{17}	0.28

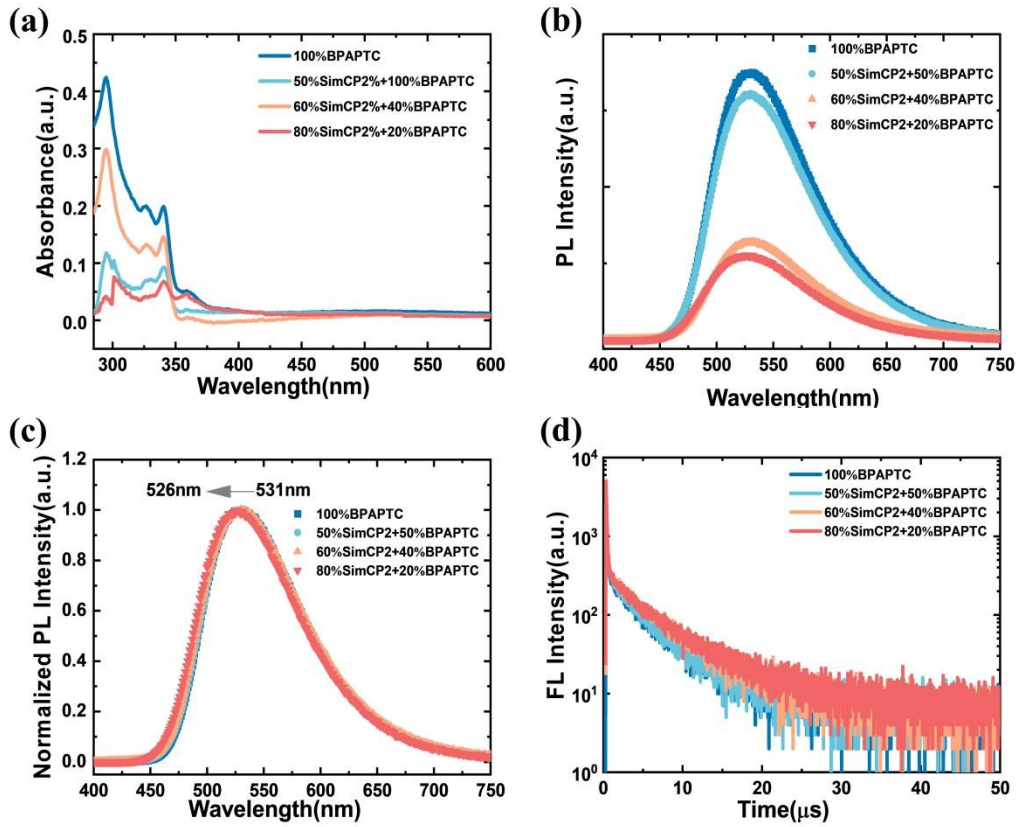

Figure S7. UV–vis absorption spectra, photoluminescence (PL) emission spectra, and PL decay curves of SimCP2+BPAPTC at different doping ratios.

5. References

[1] W. F. Pasveer, J. Cottaar, C. Tanase, R. Coehoorn, P. A. Bobbert, P. W. M. Blom, D. M. de Leeuw, M. A. J. Michels, *Phys. Rev. Lett.*, 2005, **94**, 206601.

[2] P. W. M. Blom, M. J. M. de Jong, J. J. M. Vleggaar, Electron and hole transport in poly(*p* -phenylene vinylene) devices, *Appl. Phys. Lett.*, 1996, **68**, 3308-3310.

[3] P. Mark, W. Helfrich, Space-charge-limited currents in organic crystals, *J. Appl. Phys.*, 1962, **33**, 205-215.

[4] W. Hwang, K. C. Kao, Studies of the theory of single and double injection in solids with a Gaussian trap distribution, *Solid-State Electron.*, 1976, **19**, 1045-1047.

[5] D. Abbaszadeh, A. Kunz, G. A. H. Wetzelaer, J. J. Michels, N. I. Crăciun, K. Koynov, I. Lieberwirth, P. W. M. Blom, Elimination of charge carrier trapping in diluted semiconductors, *Nat. Mater.,* 2016, **15**, 628-633.